Specific Heat of Superconducting Zn Nanowires

James S. Kurtz,* Robert R. Johnson,† Mingliang Tian, Nitesh Kumar, Zhigang Ma, Shengyong Xu,‡ and Moses H. W. Chan

Center for Nanoscale Science and Department of Physics, Pennsylvania State University, University Park, Pennsylvania 16802-6300, USA

(Received 18 November 2006; published 11 June 2007)

We present heat capacity measurements on crystalline Zn nanowires with diameters of 230 and 23 nm, bracketing the superconducting coherence length of 155 nm. Transport measurements on superconducting nanowires have found a crossover from three-dimensional to one-dimensional behavior as the wire diameter was reduced below the coherence length. In contrast, the normalized heat capacity peak of the 23 nm Zn nanowires is found to be nearly identical to that of 230 nm wires and bulk Zn, indicating their thermodynamic properties remain three dimensional.

DOI: 10.1103/PhysRevLett.98.247001 PACS numbers: 74.78.Na, 74.25.Bt

Superconductivity in quasi-one-dimensional (1D) nanowires has been studied extensively in recent years. Advances in fabrication now allow the production of high-quality wires whose diameters are smaller than the superconducting coherence length. In this regime, transverse excitations in the superconducting order parameter are energetically less favorable, and the system approaches the 1D limit where the role of thermal fluctuations is more important than in 3D. To date, focus has centered on the electrical transport properties [1–7] of these nanowires and the role that thermal and quantum phase slips play in the destruction of superconductivity. Theoretically, one expects the resistivity to be a good measure of the phase correlation of the order parameter along the entire length of the wire, though it can be quite sensitive to local details of the superconducting order parameter. There has been relatively little attention paid, however, to the global thermal properties of nanowires. In particular, specific heat measurements, which are crucial to the study of bulk superconductivity, to our knowledge, have not been performed on the 1D systems. This is the case in spite of the interesting body of work on the specific heat of "0D" superconducting particles [8–10]. Advances in electrochemical deposition now permit the synthesis of large quantities of nanowires. Transport measurements have been carried out on arrays of such nanowires, revealing 1D behavior for small diameters [4] and an intriguing antiproximity effect [5]. The central question we address in this work is to what extent does a more global, amplitude-sensitive measure of the destruction of the superconducting state in these nanowires mirror what is seen by the transport measurements. Here we present specific heat measurements on wires that, according to transport data, are deep in the 1D regime. Our results indicate, however, that the specific heat is remarkably unchanged by this level of confinement.

The samples consisted of Zn nanowires filling porous anodic alumina membranes (AAMs). The AAM containing the larger wires was commercially fabricated [11]. The smaller pore AAM was custom fabricated using procedures outlined elsewhere [12]. Distilled water, clean acids, high purity Al, and metal-free containers and implements were used in all fabrication steps to minimize magnetic contaminants in the AAM.

Scanning electron microscope (SEM) images of the AAMs are shown in the inset of Fig. 1. The custom fabricated AAM has nonintersecting pores with a narrow diameter distribution and pore density of 6.7×10^{10} pores/cm^2. Transmission electron microscope images of nanowires taken from this AAM yielded diameters of 23 ± 2 nm. The commercial, large-pore AAM had a pore density of 0.097×10^{10} pores/cm^2 with more widely distributed diameters of 230 ± 40 nm and with pore branching in some pores. The sample thicknesses, measured by SEM, were 64 and 56 μm for the small-pore and large-pore samples, respectively.

Zn wires were electroplated into the pores of AAM following procedures developed elsewhere [5]. Residual Zn on the membrane's outer surface was removed by polishing under a microscope. X-ray analysis and transmission electron microscope images of Zn wires prepared

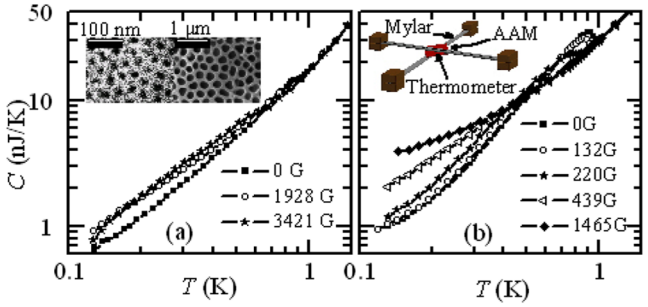

FIG. 1 (color online). Raw heat capacities at several fields for (a) 23 nm Zn nanowires and (b) 230 nm Zn nanowires. Curves at other fields have been deleted for clarity. Insets: SEM images of (a) small-pore AAM and large-pore AAM, and (b) a schematic of the Mylar-web calorimeter.

in this way revealed relatively crystalline wires, with grain size of 200 nm along the length of the wire [13]. Following the heat capacity measurements, the Zn content of the samples was determined by inductively coupled plasma mass spectrometry. Zn masses were 0.148 and 0.856 mg for the small-pore and large-pore samples, respectively.

The calorimeters [Fig. 1(b) inset] consisted of 10 mm^2 pieces of Zn-filled AAM suspended between two crossed Mylar® strips (0.8 mm × 15 mm × 2 μm) and secured with less than 0.1 mg of Apiezon® *N* vacuum grease. A 10 kΩ Au-Pd alloy heater was sputtered onto one Mylar strip near the sample. The thermometer was a SPI Supplies® conductive carbon paint film, sprayed in a fine mist onto the sample area of the second strip. This film thickness was less than 10 μm with resistance less than 10 kΩ. The heater and thermometer were connected with thick traces of sputtered Au-Pd coating the length of the strips. Cu electrodes clamped the ends of the strips, providing mechanical support and thermal and electrical contact to the leads.

Each Mylar-web calorimeter was encased in a temperature controlled, evacuated Cu cell to prevent helium adsorption. The cells were anchored through a thermal weak link to the mixing chamber of a dilution refrigerator in the center of a superconducting magnet. The calorimeters were connected to ac-Wheatstone bridges outside the cryostat by twisted, shielded pairs of electrical leads passing through microwave and radio-frequency filters anchored at the mixing chamber and radio-frequency filters anchored at the top of the cryostat. This aggressive filtering minimized spurious heating of the thermometer and allowed detection of low level signals.

Heat capacity was measured using the ''ac method'' [14]. The four Mylar strips with Au-Pd leads acted as weak links between the sample (with heater and thermometer) and the thermal bath (the Cu cell). The frequency of the applied heater power was low enough that the calorimeter was in internal thermal equilibrium with the thermometer closely tracking the sample temperature, but high enough that the ac modulation was not transmitted across the weak links. These conditions were satisfied within a broad range of frequencies (typically 0.2–5 Hz) over the entire temperature range. The heat capacity data shown below were measured at a frequency in the middle of this range, between 1 and 2 Hz.

External magnetic fields were applied parallel to the nanowires. Immediately before data collection at each field, the sample assembly was warmed to 9 K to expel trapped flux and the thermometers were recalibrated over the entire temperature range. The data showed no hysteresis between heating and cooling, and no dependence on field polarity. Typical temperature oscillation amplitude at the sample was 1% of the absolute temperature, and typical scatter in the heat capacity was less than 2% at the extremes of the temperature range and 0.2% for the bulk of the data.

The measured heat capacity is shown in Fig. 1 where a superconducting transition near 1 K is visible in the raw data for both samples. An external field causes a downward shift in the transition temperature, a broadening of the feature at the transition, and a rise in the heat capacity at low temperatures. These features are more pronounced in the large-pore sample because of the higher Zn filling fraction. The fields required to shift the transition are higher for the small-pore sample and higher in both samples compared to bulk ($H_c^{\mathrm{bulk}} = 53$ G) [15].

We estimate the Mylar sandwiching the AAM sample contributes less than 1% to the total heat capacity. The dominant contribution is the AAM. We expect the specific heat of this component will behave as a disordered insulator with large specific heat at low temperatures [16]. To determine the Zn contribution, we assume the specific heat of Zn nanowires above the superconducting transition is the same as that of bulk. This assumption is supported by measurements on several systems of small metal particles in insulating hosts [17]. Theoretical treatments of isolated superconducting particles [8] indicate that quantum size effects on the electronic specific heat are significant when the discrete quasiparticle energy level separation δ is of order $0.1k_BT$, where k_B is Boltzmann's constant. This temperature regime for 20 nm spherical Zn particles is on the order of 10 mK, much lower than the range of interest in this experiment. Long cylinders of the same diameter need to be cooled even further for quantum confinement effects to be seen. Furthermore, experimental measurements [17] on a variety of metal particles of diameters between 2 and 13 nm found little evidence of either quantum size effects or electronic surface-state effects on the normal electron specific heat.

Contributions to heat capacity due to surface states and quantum size effects have been observed in phonon systems [18]. A theory [19] for the phonon contribution based on an elastic continuum model of a small cylinder predicts a specific heat for the phonon system above T_c of $c_{\mathrm{pn}} = AVT^3 + BST^2$, where A and B are constants at low temperatures, V is the particle volume, and S is its surface area. The first term is the usual Debye expression for bulk solids, and the second term is a surface contribution. Following Ref. [18], a calculation of this surface term's size for long, 20 nm diameter wires, yields $BST^2 = 0.58T^2\ \mathrm{nJ\,K^{-1}\,mg^{-1}}$, a quantity similar in magnitude to the bulk lattice contribution [20] in Zn for our temperature range. This surface effect coexists, however, with quantum size effects, which can decrease the specific heat. Further reductions of the surface enhancement can be expected for a nanowire with surface excitations suppressed by pore wall contact. Hence, the surface contribution calculated above can be viewed as an upper estimate on the enhancement of the phonon part of the specific heat.

From the measured data at all fields above T_c we subtract the known heat capacity of bulk Zn [20]. The remainder is

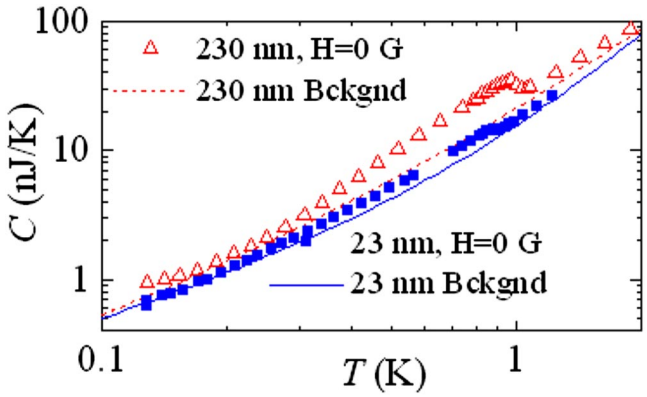

FIG. 2 (color online). Zero-field curves for both samples with their estimated background contributions.

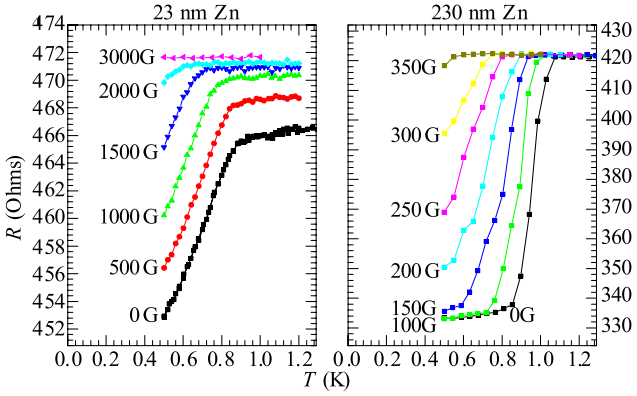

FIG. 4 (color online). Transport measurements on ensembles of 23 and 230 nm Zn wires contacted by Ag leads.

the background, composed of pure metals, alloys, and disordered insulators. The small-size enhancements to the lattice contribution, if present, would shift our background estimate by no more than 0.5% at 1 K and less at lower temperatures. We fit this data above T_c and extrapolate below 0.7 K using a three-order polynomial, which is then subtracted from all the raw data, as shown in Fig. 2 for the zero-field curves.

For nonzero fields, we subtract the same background and plot the Zn nanowire specific heat in Fig. 3. Schottky-like upward deviations at high field and low temperature for both samples are evidence of paramagnetic impurities in the alumina. The temperature and field dependence are consistent with roughly 5 and 50 ppm of spin-1/2 impurities in the small-pore and large-pore samples, respectively. This effect was stronger before stringent precautions were taken to minimize magnetic impurities in the AAM and nanowires. Despite the higher concentration in the commercial alumina, the lower fields applied to that sample keep the effect small and confined to low temperatures.

The critical temperature in zero field, defined as the midpoint of the jump, for both samples is higher than in bulk ($T_c^{\text{bulk}} = 0.85$ K [20]): 0.89 and 0.94 K for the small-pore and large-pore samples, respectively. Transition temperatures from transport measurements (see Fig. 4) on similarly prepared samples more closely agree with the high-temperature *onset* of the heat capacity jump (0.89 and 1.05 K, respectively), though both measurements consistently yield a larger transition temperature for the larger wires. The enhancement of the transition temperature may be due to local disorder (samples are polycrystalline with a mean free path $l = 12$ and coherence length $\xi_o = 155$ nm determined by previous transport measurements [5]), though it is unclear why the larger wires are more affected.

To compare the height and breadth of the transition we plot in Fig. 5 the zero-field specific heat, normalized to the specific heat of the normal state just above T_c, against the reduced temperature. Because of uncertainties in the background subtraction for the data in Fig. 5, there is a systematic uncertainty in magnitude of roughly 10%. The specific heat jump of bulk Zn crystal is slightly sharper than that of

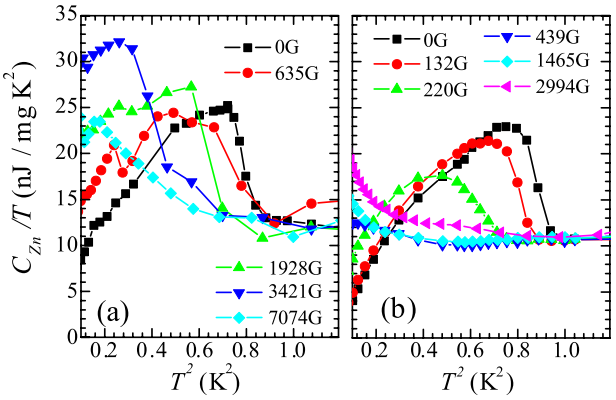

FIG. 3 (color online). Specific heat of Zn nanowires in several fields with background subtracted for (a) the small-pore sample and (b) the large-pore sample. Curves at other fields have been deleted for clarity.

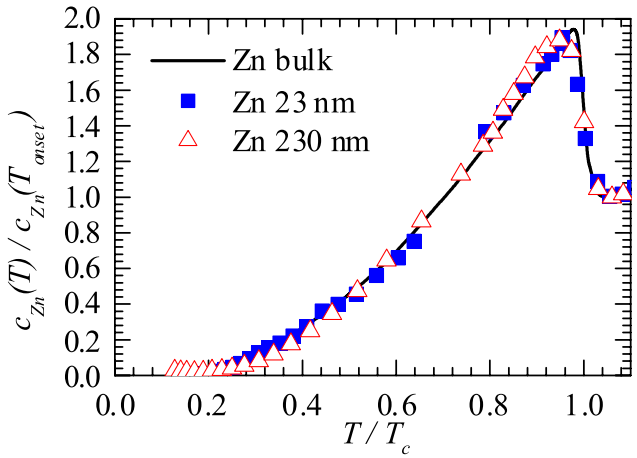

FIG. 5 (color online). Normalized specific heat versus normalized temperature. The solid curve is bulk Zn data.

these samples, as measured by the temperature difference between the local specific heat minimum and maximum near the transition. The spread in wire diameters in each sample and the dependence of the transition temperature on wire diameter can account for much of this width. The more rounded peak of the large-pore sample would thus be consistent with its larger spread in wire diameter. The height and breadth of the specific heat jump are virtually unaffected by the severe confinement, which is the central result of this work.

In contrast to this result, the situation for 0D particles is quite different. Muhlschlegel *et al.* [8] used a generalized Ginzburg-Landau (GL) approach to calculate the effect of thermodynamic fluctuations of the order parameter on the specific heat of a small, isolated superconducting particle. For progressively smaller particles the critical region widens and uniformly smooths out the sharp, bulk specific heat discontinuity. They estimated that for BCS particles of order 20 nm in diameter, the electronic specific heat jump could be just half the size of that in bulk, with significant rounding and broadening of the transition. Experimental work on Sn particles [10] verified these predictions. Broadening of the transition region over a range of $0.1T/T_c$ was observed for diameters as large as 51 nm. For 18 nm particles the transition region spanned $0.4T/T_c$. The signature of superconductivity was virtually absent for 7 nm particles. Thus, 0D effects due to thermal fluctuations were already easily observable for particles only 4 times smaller than the bulk coherence length of 200 nm.

In the case of 1D wires, we also expect that in the limit of small diameters the superconducting order will be destroyed. Theoretical and numerical work [21–24] in generalizing the 1D GL problem to account for fluctuations has been done to determine the specific heat in the critical region. It was found that a broadening of the transition with a very weak specific heat peak in the transition region occurs, unlike the 0D case. An approximate expression for the width of this temperature region was given [24], yielding roughly 200 mK for the case of 20 nm Zn wires with a 12 nm mean free path and 2 μm bulk coherence length.

For the Zn nanowire specific heat presented here, there is little evidence of such broadening of the transition region. These results indicate a robust specific heat signature in 20 nm wires compared to bulk and to similarly prepared, but thicker, nanowires. This sets a limit on the role of fluctuations in these nanowires. Evidently, the diameters must be much smaller than 20 nm before local superconducting order is substantially destroyed by thermal fluctuations.

In conclusion, these measurements are the first to probe the thermodynamics of superconducting nanowires with diameters well below the coherence length, providing a new perspective on quasi-1D nanowires. Whereas truly 1D phenomena such as phase slips have been readily observed by transport measurements, similar wires exhibit no observable 1D behavior in the thermodynamic data. Instead, we see an essentially bulklike signature in the specific heat. Evidently, the suppression of superconducting order by thermodynamic fluctuations is much more sensitively detected by electrical transport, since a zero-resistance state depends on long-range phase coherence along the entire length of the sample. Specific heat, on the other hand, probes more local superconducting order, which is apparently still quite robust even in 23 nm diameter nanowires that are nearly 7 times smaller than the coherence length.

This work was supported by NSF Grant No. 213623 and REU Grant No. 0353890.

*Electronic address: kurtz.james@gmail.com
†Present address: Department of Physics and Astronomy, University of Pennsylvania, Philadelphia, PA 19104, USA.
‡Present address: Department of Electronics, Peking University, Beijing 100871, China.

[1] N. Giordano, Phys. Rev. Lett. **61**, 2137 (1988); N. Giordano, Physica (Amsterdam) **203B**, 460 (1994).
[2] P. Xiong *et al.*, Phys. Rev. Lett. **78**, 927 (1997); F. Sharifi *et al.*, Phys. Rev. Lett. **71**, 428 (1993).
[3] A. Bezryadin *et al.*, Nature (London) **404**, 971 (2000).
[4] M. L. Tian *et al.*, Phys. Rev. B **71**, 104521 (2005).
[5] M. L. Tian *et al.*, Phys. Rev. Lett. **95**, 076802 (2005).
[6] M. Zgirski *et al.*, Nano Lett. **5**, 1029 (2005).
[7] F. Altomare *et al.*, Phys. Rev. Lett. **97**, 017001 (2006).
[8] B. Muhlschlegel *et al.*, Phys. Rev. B **6**, 1767 (1972).
[9] T. Worthington *et al.*, Phys. Rev. Lett. **41**, 316 (1978); R. L. Filler *et al.*, Phys. Rev. B **21**, 5031 (1980).
[10] N. A. H. K. Rao *et al.*, Phys. Rev. B **29**, 1214 (1984).
[11] Purchased from VWR, labeled Anodisc 25 (0.02 μm nominal pore diameter).
[12] M. L. Tian *et al.*, Nano Lett. **5**, 697 (2005).
[13] J. G. Wang *et al.*, Nano Lett. **5**, 1247 (2005).
[14] P. Sullivan *et al.*, Phys. Rev. **173**, 679 (1968).
[15] C. Kittel, *Introduction to Solid State Physics* (John Wiley & Sons, New York, 1996), 7th ed.
[16] K. Nielsch, Nano Lett. **2**, 677 (2002); S. Shingubara, Nanopart. Res. **5**, 17 (2003).
[17] W. P. Halperin, Rev. Mod. Phys. **58**, 533 (1986).
[18] V. Novotny *et al.*, Phys. Rev. Lett. **28**, 901 (1972); V. Novotny *et al.*, Phys. Rev. B **8**, 4186 (1973).
[19] M. Dupuis *et al.*, J. Chem. Phys. **33**, 1452 (1960); A. Maradudin *et al.*, Phys. Rev. **148**, 945 (1966).
[20] G. Seidel *et al.*, Phys. Rev. **112**, 1083 (1958); T. C. Cetas, Phys. Rev. **182**, 679 (1969).
[21] V. V. Shmidt, Pis'ma Zh. Eksp. Teor. Fiz. **3**, 141 (1966) [JETP Lett. **3**, 89 (1966)].
[22] S. Marcelja, Phys. Lett. A **35**, 335 (1971).
[23] L. W. Gruenberg *et al.*, Phys. Lett. A **38**, 463 (1972).
[24] D. J. Scalapino *et al.*, Phys. Rev. B **6**, 3409 (1972).